JOURNAL OF PHYSICAL CHEMISTRY A (ISSN: 1089-5639) (eISSN: 1520-5215) 2015: Paper 10.1021/jp510202r. (2015)

DOI: 10.1021/jp510202r

A Quasiclassical Trajectory Study of the Reaction of H Atoms with $O_2(^1\Delta_g)$

Péter Szabó[1] and György Lendvay[1,2]*

[1]Department of General and Inorganic Chemistry, Institute of Chemistry, University of Pannonia, P.O.B. 158, Veszprém H-8201, [2]Institute of Materials and Environmental Chemistry, Research Centre for Natural Sciences, Hungarian Academy of Sciences, Budapest, Magyar Tudósok krt. 2., H-1117 Hungary

Abstract The kinetic and dynamic characteristics of the reaction of H atoms with electronically excited O_2 were studied using the quasiclassical trajectory (QCT) method and the potential energy surface of Li *et al*. (*J. Chem. Phys*. **2010**, *133*, 144306-144314.). The reaction takes place via a deep potential well that can be entered by climbing a barrier in the reactant valley and can be left without a barrier on the product side. In this reaction the basic assumptions of statistical rate theories are not fulfilled: i) 80% of the trajectories cross the barrier region twice and are nonreactive; b) The energy is not equilibrated in the HO_2 potential well. The QCT cross sections agree well with those from the existing exact quantum mechanical data and extend them to vib-rotationally excited reactants. The thermal rate coefficients agree well with measurements of pure reactive quenching of $O_2(^1\Delta_g)$ and are

lower than those involving both reactive and electronic quenching. The temperature dependence is described as $k_2 = 5.81\times10^{-16}\ T^{1.45}\ \exp(-2270/T)$ cm^3 molecule^{-1} s^{-1}. Based on comparison of the QCT data with the two kinds of experiments we estimate that electronic quenching is faster than reaction by a factor of about 10 at low and 2 at high flame temperatures.

Keywords: combustion acceleration; singlet molecular oxygen; reaction dynamics; transition state theory; complex formation.

INTRODUCTION

The reaction of H atom with dioxygen has been termed "the single most important" elementary step in combustion[1]. Its importance comes from the fact that it is a chain-branching step, yielding two active species, O atom and OH radical starting from one, the H atom. This is the step that introduces O_2 into the chain of reactions. At high pressures the HO_2 intermediate is collisionally stabilized making the reaction a chain-termination step. Due to its importance, the reaction has been the subject of a large number of studies, both experimental and theoretical.[2,3,4,5,6,7,8,9,10,11,12,13,14,15,16,17,18,19,20,21,22,23,24,25,26,27] A large body of information is available on the reaction of H atoms with oxygen molecules in the electronic ground state,

$$H(^2S) + O_2(^3\Sigma_g^-) \rightarrow O(^3P) + OH(^2\Pi_g). \qquad \text{(R1)}$$

Both the kinetics and the dynamics of the reaction, including collisional energy transfer are quite well established. Much less is known about the reaction of singlet molecular oxygen, $O_2(^1\Delta_g)$ with H atoms,

$$H(^2S) + O_2(^1\Delta_g) \rightarrow O(^3P) + OH(^2\Pi_g) \qquad \text{(R2)}$$

This reaction seems also to be feasible in the higher stratosphere and in high-temperature flames. Application of excitation of molecular oxygen to the singlet state was proposed as a way to accelerate combustion already decades ago.[28] Electronically excited oxygen will not necessarily be present in flames even at high temperatures, but it is produced in almost all oxygen-containing plasmas, because the energy needed to excite $O_2(^3\Sigma_g^-)$ is relatively low (94.5 kJ/mol)[29]. The radiative lifetime of $O_2(^1\Delta_g)$ is relatively long (>3800 s)[30], so that it can live long enough in flames to perturb the kinetics of combustion if it proves to be reactive enough. It is known that the barrier on the potential energy surfaces of its reactions with closed-shell molecules is high, but it can easily react with open-shell reactants. Both the experiments in which the reaction mixture was directed to pass through an electric discharge and the related combustion modeling studies[31,32,33,34,35,36] demonstrated that the concept works: the flame velocity was found to increase in the presence of electronically excited dioxygen.

Several experimental studies[37,38,39,40,41,42] have been reported about the kinetics of the reaction of $O_2(^1\Delta_g)$ and hydrogen atoms. Early work[37,38] resulted in estimates of the rate coefficient. Schmidt and Schiff[39] followed the $O_2(^1\Delta_g)$ concentration to get the rate of loss due to collisions with H atoms at room temperature and obtained a rate coefficient of 2.5×10^{-14} cm^3 $molecule^{-1}$ s^{-1}. The technique they used does not allow distinction between chemical reaction and physical quenching. Cupitt *et al*.[40] measured the rate at several temperatures between 300 and 430 K and argued that chemical reaction dominates in the process. The Arrhenius parameters they derived are shown in Table 1. Basevich and Vedeneev[41] did similar experiments at higher temperatures (500-800 K). The corresponding Arrhenius parameters differ from those of Cupitt *et al*.,[40] the activation energy being more than 50 % higher. Several years later, Popov[31] combined the rate coefficients measured in both studies, and found the measured points to lie along essentially the same line in the Arrhenius

representation. The Arrhenius parameters he derived (Table 1) have been widely used in flame simulations.

The latest reported experiments were performed by Hack and Kurzke[42] who showed that the rate of reaction (R2), with or without physical quenching, cannot be determined if only the concentration of the reactants is monitored. They derived the rate coefficients of the pure chemical step, (R2) by following the concentration of H and O atoms as well as OH radicals and fitting a complex model including about 20 reactions to the measured data. The values they obtained in the temperature range of 299-423 K are smaller by about an order of magnitude than those measured by Cupitt *et al*.,[40] indicating that the reactive rate is below 10% of the total rate of $O_2(^1\Delta_g)$ removal. Note that under the conditions of the Hack and Kurzke experiment, the possible loss of $O_2(^1\Delta_g)$ is negligible because of the small initial H atom concentration so that physical quenching, if occurs, does not influence of the radical concentration profiles.

Early theoretical studies were based on the assumption that the activation energy of the reaction of singlet molecular oxygen can be derived from that of the reaction of ground-state oxygen from a simple curve-crossing model[43]. This view seems to be oversimplified in the light of the recent calculations of the potential energy surface (PES) of the reaction by high-level electronic structure methods by Li *et al*.[44] In Fig. 1, shown are the major features of the excited-state PES, compared with those of the ground-state reaction. There is a deep potential well corresponding to HO_2 on both PES. The two potential surfaces are degenerate on the product O + OH side. However, there are some qualitative differences between the PES for the two electronic states. The reaction of $O_2(^3\Sigma_g^-)$ is endothermic and displays no barrier either in the entrance or the exit channel. The excited-state reaction is exothermic but there is a barrier in the entrance valley and none in the exit valley. This indicates that the dynamics and accordingly, the kinetics of the two reactions can be expected to show significant

differences. Due to the presence of both a well (making possible the formation of long-lived complexes) and a barrier on the PES, the most reliable way of estimating the rate coefficient of the reaction is through reaction dynamics calculations. The potential energy surface (PES) needed for dynamical studies were developed by Li *et al.*[44] who calculated the potential energy at some 17,000 points, and made a spline fit to the calculated points. Using the PES the basic dynamical properties of the reaction were calculated[45] for the ground vibrational and rotational state of $O_2(^1\Delta_g)$ using accurate quantum mechanical methods. Reliable calculation of the thermal rate coefficient from the theoretically derived reaction cross sections, however, was not possible because of the limited range of initial conditions.

Expected dynamical behavior based on the properties of the potential energy surface

The investigation of the topology of the potential surface developed by Li *et al.* [44] allows one to estimate the qualitative features of the dynamics of the reaction. Sections of the potential energy surface are shown in Fig. 2, where the potential energy is plotted as a function of the location of the H atom in the triatomic plane with respect to the center of mass of the O_2 molecule. The O–O distance is set to: 1.1 Å, the inner turning point of the ground vibrational state of $O_2(^1\Delta_g)$, 1.2 Å, the equilibrium bond length of O_2, 1.4 Å, the equilibrium O-O distance in electronically excited HO_2 and 1.8 Å which corresponds to a more-or-less separate pair of an OH radical and an O atom. Note that the PES is cylindrically symmetric around the O–O axis. One can see that a repulsive wall protects the O_2 molecule at the two ends as well from sideways attack. There is a relatively narrow band around both oxygen atoms where the H atom can approach the molecule. As expected for an exothermic reaction, the barrier is early, the 31.7 kJ/mol-high saddle point is in the entrance valley, but already almost at the same Jacobi angle as that corresponding to the equilibrium geometry of $HO_2(A')$. The potential well is actually spread to two tori around the O atoms that correspond to the HOO' as well as HO'O isomers, respectively. The electronically excited HO_2 can isomerize without

decomposition, the barrier being -94 kJ/mol at R_{OO} = 1.398 Å below the H + O_2 asymptote. The location of the entrance barrier in the reactant valley is more clearly visible in Fig. 3, showing the PES as a function of the length of the forming and breaking bonds, at the H–O–O angle being fixed at 112.4° corresponding to the saddle point geometry (where the O–O and O–H distances are 1.24 Å and 1.685 Å, respectively). From the features of the PES one can expect that the reactivity of O_2 will depend on its rotational excitation: the cone of acceptance covering the two reactive bands around the O_2 molecule is expanded when the molecule rotates and the bands sweep almost a complete sphere when O_2 rotates. According to Polanyi's rules[46], vibrational excitation would not be efficient to increase the chance for the system to enter the HO_2 well. One can also expect that the stripping-type reactions will involve rotational excitation of the product OH because at the favorable direction of approach the O-O-H arrangement is bent. The distribution of the reaction energy among the product degrees of freedom is not easy to predict because it will depend on the time spent in the potential well.

The purpose of the present work is to derive ab initio the thermal rate coefficient for reaction (1). To this end we extend the range of the initial conditions, in particular, the number of initial rotational states considered as compared with the earlier dynamics calculations. The purpose is include in the thermal averaging the high rotational states of O_2 whose population is significant at flame temperatures. We use the quasiclassical trajectory (QCT) methodology, which – after "calibration" against the existing quantum dynamical data – allows us not only to get the excitation functions needed for rate coefficient calculations, but also provides some insight into the dynamics of reactions on potential surfaces involving a deep potential well with an entrance but no exit barrier.

The rest of the paper is organized as follows: after providing a summary of the methodology, we show the calibration of the QCT method, then present the results on the

effect of vibrational and rotational excitation of the reactants on the dynamics of reaction (R2), followed by the product state distributions and the thermal rate coefficients. Then we discuss the results on the microscopic dynamics of the reaction.

METHODS

The quasiclassical trajectory calculations were performed using an extensively modified version of the VENUS code[47]. 2×10^5 trajectories were calculated at each collision energy. For the integration of Hamilton's equation of motion in Cartesian coordinates, the sixth-order Adams-Moulton predictor-corrector algorithm initiated by a fourth-order Runge-Kutta integrator was used. The step size of 0.1 fs was employed for integration. The conservation of the total energy was better than 0.05 kJ/mol. The initial H–O_2 separation was fixed at 9 Å that guarantees a negligible initial interaction between H and O_2. Based on calculations of the opacity function at several collision energies and O_2 initial quantum states, the maximum impact parameter was set to b_{max} = 3.0 Å. When the impact parameters are Monte Carlo sampled so that the number of trials in different impact parameter domains is proportional to the impact parameter, the initial state selected reaction cross section is given by

$$\sigma_r\left(E_{coll}, v, j\right) = \pi b_{\max}^2 \frac{N_r\left(E_{coll}, v, j\right)}{N}, \qquad (1)$$

where b_{max} is the maximum impact parameter, N_r is the number of reactive and N the total number of trajectories, v and j denote the initial vibrational and rotational quantum numbers of the reactant molecule and E_{coll} is the relative collision energy of reactants. In the evaluation of trajectories we tested several commonly used techniques, including:

1. QCT: all reactive trajectories included in the calculation

2. QCT-ZP: trajectories producing OH with smaller than 0 vibrational quantum number are discarded without replacement

3. GW-QCT: trajectories are considered with a Gaussian weight depending on the distance of the final classical action variable of the product molecule from the nearest quantum state.[48,49,50] We use the standard value of 0.05 for the width of the Gaussian "window."

We also recorded the fate of nonreactive trajectories that entered the potential well by recording if the trajectory entered the region of the configuration space where the energy is below one half of the dissociation energy to O + OH which is at 96.7 kJ/mol below the reactant level. All such trajectories necessarily pass the potential barrier and represent a very conservative estimate of the fraction of trajectories that, after crossing the barrier in the forward direction will cross it again in the reverse direction.

RESULTS

A. Validation of QCT calculations Ma *et al*.[45] performed exact quantum scattering (EQ) calculations on the A' PES. They studied the reaction starting from the ground vibrational and rotational state of $O_2(^1\Delta_g)$ in the collision energy range (20-90 kJ/mol). QCT calculations were performed in the same energy range for the same quantum state to evaluate the performance of the three ways of handling final vibrational states. The results are shown in. Fig. 4 (Fig. S1 shows the threshold region magnified). The QCT-ZP method considerably underestimates the EQ cross sections. The simple QCT and the GW-QCT methods provide very similar cross sections that match excellently those obtained in the exact quantum scattering calculation (except the sudden rise in the threshold region). We consider this a validation of the simple QCT and the GW-QCT methods and assume that it can be reliably used to predict the dynamical details of the reaction outside the region covered by the exact quantum mechanical method. Hereinafter only the results obtained with the GW-QCT method are presented. It is worthwhile mentioning that the barrier very probably is passed with minimal assistance from vibration (see below). This means that in a system with a

barrier before and no barrier after a potential well, the common reasoning that zero-point energy violation in the products is an indicator of non-quantum effects in the reaction loses sense and omission of trajectories yielding products with less than zero-point energy will lead to misleading results.

B. Integral cross sections The GW-QCT excitation functions for various vib-rotational states of $O_2(^1\Delta_g)$ are presented in Fig. 5 (and Fig. S2, zoomed on the threshold region). The integral cross sections are monotonic functions of the collision energy. The threshold energy is 28.9 kJ/mol at $v = 0$ and $j = 0$. The sum of this collision energy and the zero-point energy of the oxygen molecule is 38.1 kJ/mol, 6.4 kJ/mol higher than the entrance channel barrier (31.7 kJ/mol). This indicates that probably only a small fraction of trajectories pass the barrier at the price of zero-point violation, which is in agreement with the early position of the barrier. Investigation of the effect of vibrational excitation on the cross sections further supports the lack of vibrational nonadiabaticity of classical trajectories near the potential barrier. Vibrational excitation of O_2 to $v = 1$ and $v = 2$ reduces the threshold energy by only 3 and 4 kJ/mol, respectively. Furthermore, surprisingly, above the $v = 0$ threshold up to $E_{coll} = 110$ kJ/mol the reaction cross sections are smaller if O_2 is vibrationally excited. Rotational excitation of the singlet oxygen molecule up to $j = 20$ does not change the cross sections except at collision energies very close to threshold, reducing the latter by about 1 kJ/mol. At higher excitation the threshold energy is further reduced with increasing j, by about 5 kJ/mol at $j = 40$ and 8 kJ/mol (wrt. the ground rotational state) when $j = 60$, and the cross sections are also larger at individual collision energies. The reduction of threshold is about 10 times smaller than the rotational energy indicating that the rotation of O_2 only marginally facilitates the system when crossing the barrier.

The threshold energy from exact quantum scattering calculations is 21.2 kJ/mol for the reaction of the vib-rotational ground state of $O_2(^1\Delta_g)$, above which the cross sections remain very small until the classical threshold energy where it starts to increase so that the EQ and QCT excitation functions in fact overlap. Considering this and the lack of zero-point energy violation, one can conclude that the reaction proceeds through tunneling at collision energies between 21 and 31 kJ/mol. Comparison with the excitation function calculated quantum mechanically for the reaction of O_2 in electronic ground state with H shows significant enhancement of the reactivity of O_2 towards H atoms by electronic excitation. The threshold energy for the reaction of triplet O_2 is 57.9 kJ/mol, much larger than in the excited state. In addition, the magnitude of the ground-state cross sections is smaller by about an order of magnitude at identical collision energies than the excited-state ones. Both these factors indicate that the reactivity of electronically excited O_2 towards H is much larger than that of triplet molecular oxygen and one can expect this will be reflected in the rate constants.

C. Differential cross sections Product angular distributions in the c.m. frame are shown in Fig. 6. (note that the scale is arbitrary but the magnitude reflects the overall reactivity). Forward-backward symmetry is observed at low collision energies, which is a signature of statistical behavior. At high collision energies dynamical effects, as expected, are found to be more significant: the forward peak increases, indicating the increasing role of stripping trajectories. Vibrational excitation of O_2 has no significant effect on the angular distribution. Rotational excitation, on the other hand, leads to a reduction of the forward and backward peaks and an increasing role of sideways scattering. In contrast, no well defined forward and backward peaks can be seen in the angular distributions of nonreactive trajectories that enter the potential well (Fig. S3). Signs of preferentially backward scattering are visible but sideways scattering is also remarkable which is in agreement with the features of the PES: the barrier in the entrance channel is at a bent arrangement.

D. Product state distributions The products are formed in relatively high rotational states already at low collision energy. The increase of the collision energy induces enhanced product rotational excitation. The vibrationally resolved product rotational distributions are shown in Fig. 7. OH is formed either vibrationally or rotationally excited. With increasing collision energy more vibrational channels open, but the shape of the rotational distribution remains almost the same. Remarkably, the distributions provided by the GW-QCT method are in excellent agreement with the exact quantum scattering data. Both (de facto identical) dynamical results deviate from the statistical distribution (amply discussed in Ref. 45) indicating that the complex does not behave statistically. On the other hand, from the distributions starting from excited rotational states (Fig. S4), there seems not to be any preference for conserving rotational energy, which is probably the consequence of the significant difference in the moments of inertia of the reactant and product diatomics.

THERMAL RATE COEFFICIENTS

The rotational and vibrational state-resolved reaction rates are calculated from the excitation functions according to Eq. (2)

$$k(T,v,j) = \left(\frac{8}{\pi\mu}\right)^{1/2}\left(\frac{1}{k_B T}\right)^{3/2}\int_0^\infty \sigma(E_{coll},v,j)E_{coll}exp\left[-\frac{E_{coll}}{k_B T}\right]dE_{coll} \qquad (2)$$

where $\sigma(E_{coll},v,j)$ is the state-resolved cross section, E_{coll} the collision energy, k_B the Boltzmann constant and μ is the reduced mass of the collision partners. The initial state resolved excitation functions were derived from trajectory calculations at v = 0, 1, and for all even-j rotational states of O_2 from j = 0 to j = 60. (Note that $O_2(^1\Delta_g)$ has only even quantum states due to nuclear symmetry.) These very large rotational quantum numbers are needed when thermal averages of j-specific rate coefficients are calculated: Due to the large moment of inertia of O_2, the Boltzmann weight of the highly excited rotational states is not negligible

at flame temperatures. For example, above 1000 K the population of rotational levels is significant up to j = 40 and even j=60 is desirable to be included in the averaging.

Representative initial j–resolved rate coefficients are shown in Fig. 8. At room temperature, rotational excitation of the oxygen molecule to j = 40 increases the rate coefficient by a factor of 5.6 which drops to 1.6 at 1000 K. The j-averaged rate coefficients are close the value of the rate of j = 10 at all temperatures, and are larger than the j = 0 values by a factor of 1.6 at 300 K and 1.2 at 1000 K.

Vibrational excitation of O_2 slightly reduces the reaction cross section and, accordingly, slows down the reaction. This minor hindrance is only observable around 1000 K where the v = 1 state of O_2 has appreciable Boltzmann-weight.

To obtain more reliable thermal rate coefficients, we introduce tunneling correction of the vibrationally and rotationally resolved excitation functions as follows: For the reaction of the vib-rotational ground state of $O_2(^1\Delta_g)$, the EQ excitation function was used at low energies until it first crossed the QCT one. Above that energy the QCT cross sections were used in the rate coefficient calculation. For the description of tunneling at higher j and v, the same fragment of the quantum scattering excitation function was applied in a similar way to modify the classical excitation function (i.e., the same tunneling behavior was assumed for each quantum state). Namely, for the vib-rotational ground-state reaction the EQ excitation function first crosses the QCT one at E_{coll} =32.8 kJ/mol, σ = 0.0335 Å^2. For excited vib-rotational states of $O_2(^1\Delta_g)$, the section of the EQ excitation function between E_{coll} = 22 kJ/mol (the EQ threshold) and 32.8 kJ/mol was shifted along the E_{coll} axis until its right-hand end matched the σ = 0.0335 Å^2 value of the relevant QCT excitation function (Fig. 9). Below that energy the QCT cross sections were replaced by the EQ ones. This correction is based on the quantum mechanical *reactive* flux, so below σ = 0.0335 Å^2 it covers all quantum effects

including not only underbarrier tunneling but also quantum effects corresponding to barrier recrossing. It should be noted that these contributions cannot be separated.

The tunneling corrected thermal reaction rate coefficient averaged over the Boltzmann distribution of initial rotational and vibrational states is shown in Fig. 10 together with the experimental data (Fig. S5 shows the *j*-dependent tunneling-corrected rate coefficients). The rate coefficient including the tunneling correction as described above is 1.34×10^{-15} $cm^3molecule^{-1}s^{-1}$ at 300 K, 1.31×10^{-12} $cm^3molecule^{-1}s^{-1}$ at 1000 K and 1.18×10^{-11} $cm^3molecule^{-1}s^{-1}$ at 2000 K. (The enhancement of the thermally averaged rate coefficients due to tunneling is a factor of 9.3 at 300K and 1.3 at 1000K.) The calculated values are closer to the measured data of Hack and Kurzke[42] than to those of the experiments where reaction and electronic quenching was not separated. The deviation from the Hack and Kurzke rate coefficients is only a factor of 1.2 at the lowest and 3 at the highest measured temperature. The average Arrhenius activation energy (Table 1.) for the rate constants thermally averaged over the initial states is 24.4 kJ/mol, larger than that proposed by Hack and Kurzke but is close to that derived by Popov[31] from the measurements including quenching and chemical reaction.

Comparison of the rate coefficients for the reaction of H atoms with $O_2(^1\Delta_g)$ and with $O_2(^3\Sigma_g^+)$ shows that electronic excitation enhances the reactivity of O_2 towards H. At low flame temperatures the rate coefficient for reaction of excited $O_2(^1\Delta_g)$ is 4 or 5 orders of magnitude higher than for $O_2(^3\Sigma_g^+)$, while at 1000 and 2000 K the difference is a factor of about 13 and 3, respectively. This is in good agreement with the observation that the presence of $O_2(^1\Delta_g)$ speeds up flame propagation. If one accepts that the rate coefficients measured by Cupitt *et al.*[40] and by Basevich and Vedeneev[41] include both reactive and nonreactive quenching, then from the ratio of these experimental rate constants (interpolated using the formula derived by

Popov) to those derived from the QCT calculations one can estimate that nonreactive quenching is 3 to 12 times faster than the chemical reaction.

It is interesting to note that as long as the conditions in flames ensure thermal equilibrium between ground-state and singlet molecular oxygen, the population of the latter is about 0.1%, 0.6% and 1.9% at 1500, 2000 and 2500 K, respectively. As long as these equilibrium populations hold in shock tubes where the experimental rate coefficients for (R1) were obtained, the measured data contain respectively a 0.5%, 1.9% and 4.7% contribution from (R2). This is much smaller than the experimental error bar, so there is no need to make a correction. It can also be noted that, although at high temperatures the contribution of (R2) to the thermal average rate of (R1) and (R2) increases quickly (it would achieve 30% at 5000 K), it will never be larger than that of (R1) because at high temperatures the latter is also very fast,

DISCUSSION

The potential surface of reaction (R2) has a unique feature: there is a potential barrier in the entrance channel, which is followed by a deep potential well on the way to products. The dynamics of this type of reaction has not been widely studied. A number of interesting questions arise for this combination of PES features such as 1) do Polanyi's rules[46] hold for such reactions or not; 2) how does the formation of the complex after passing the entrance barrier (with energies significantly above product channel energy) influence the dynamics of the reaction; 3) is the behavior of the complex formed statistical or not, including 4) whether the state distribution of nonreactive trajectories that entered the complex region shows signs of complex formation and 5) whether the barrier is re-crossed by a significant fraction of trajectories that pass it in the forward direction.

Concerning Polanyi's rule, the basic piece of information is that the potential barrier is in the reactant valley. From this one can expect that vibration is not the preferred degree of freedom

for promoting the reaction. In accord with this expectation, in the dynamical studies the threshold energy for reaction of singlet O_2 was found to be essentially the same with or without vibrational excitation of the reactant. At energies above threshold, the reactive cross sections for $v = 1$ are somewhat lower than those at $v = 0$ at identical collision energies. This shows that in inducing reaction, vibrational energy is much less effective than translation. If the reaction cross sections are plotted against the sum of vibrational and translational energy, the excitation function for $v = 1$ is shifted to higher energies with respect to that corresponding to $v = 0$ by the amount of the energy in vibration (17.7 kJ/mol for $v = 1$, with respect to z.p.e.). All these facts indicate that the dynamics of the reaction follow Polanyi's rule. However, one has to keep in mind that passing the barrier does not necessarily means the trajectory will be reactive; it only guarantees that the system enters the potential well. The number and behavior of possible trajectories that enter the well but cross again and depart as nonreactive is a key factor in characterizing the dynamics of this system.

When one monitors the potential energy of individual trajectories, they turn out to pass the barrier region with a potential energy hardly exceeding the saddle point energy (generally by not more than a few kJ/mol) when the O_2 initially is in the vibrational ground state. The spread is larger when $v = 1$ or 2, but this can be understood to be a consequence of the larger amplitude of the oscillation around the minimum energy path. This also suggests that for vibrationally ground-state oxygen, the system does not need to borrow energy from vibration to pass the barrier, even though the latter is at the early part of the curvature of the minimum energy path. From this it follows that for this reaction, zero-point violation at barrier crossing as a classical artifact is of limited importance and would probably not lead to a significant reduction of the threshold energy. This means that the reason why QCT-ZP reaction cross sections are lower than the simple QCT (or GW-QCT) ones is not the ZPE violation at barrier crossing. Instead, many trajectories, after entering the HO_2 potential well without vibrational

energy leakage undergo some vibrational energy redistribution and emerge on the product side as OH with less that zero-point energy.

To understand the details of the dynamics, we monitored trajectories that enter the deep part of the potential well, i.e. H and O_2 form a complex. To this end we recorded the trajectories that access the region of the configuration space where the potential energy is one half of the dissociation energy of the complex to O + OH (138 kJ/mol below the reactant level). The number of collisions getting into this region will provide a very conservative estimate on the rate of complex formation. This is in fact a capture model (the classical analog of the quantum capture theory used by Ma et al.). What is more in our QCT calculations is that in our model, dynamics is partly introduced by following the trajectories even after capture. This enables us to tell apart reactive and nonreactive captured trajectories. The cross section of complex formation (including both reactive and nonreactive collisions) is plotted against the collision energy in Fig. 11 (and Fig. S6 zoomed at the threshold region). The threshold for entering the potential well is the same for reactive and nonreactive collisions and the ratio of reactive to complex-forming nonreactive cross sections remains constant when the collision energy increases. About four times more trajectories leave the complex in the reactant direction than towards products. This means that about 80% of trajectories cross the barrier at least twice, once from the reactant side and once in the opposite direction (the chance of passing it more than twice is negligible). This holds not only at high collision energies but also in the threshold region. Based on this one can conclude that one of the basic assumptions of transition state theory, the existence of a "point of no return" is not fulfilled for this reaction: One can not find a dividing surface in the barrier region that satisfies the condition that no trajectory crosses it more than once. The observations made using quasiclassical trajectories are in good agreement with the earlier quantum statistical[51,52] calculations[44,45] which were found to overestimate the reaction cross sections by a factor of 2.3. (A possible

explanation for the difference in the numerical values of the factors is that the two models use different definitions for capture.)

Further information can be gained from the lifetime distribution of the collision complexes. Exponential lifetime distribution characterizes complexes that decay completely randomly,[53] in other words, the phase space points are uniformly accessible. This is one of the conditions for the applicability of statistical theories of reaction rates to the decomposition of the complex. The lifetime of the collision complex was calculated as a classical analog to Smith's collision lifetime matrix[54]: the lifetime is the delay caused by the interaction as compared to an inelastic hard-sphere collision. The lifetime then is obtained from the total duration of the collision by subtracting the time of inbound flight from the initial center-of-mass separation to 3 Å and the analogous outbound flight time.

The lifetime distributions of the reactive and the complex-forming nonreactive trajectories are shown in Fig. 12 for various sets of initial conditions. In the reaction of $O_2(^1\Delta_g)$ in its vib-rotational ground state, at low collision energies the contribution of prompt reactive trajectories is small. This means that if the barrier is passed with a small excess translational energy, a significant time, about 0.5 ps is needed for the system to find its way out in the product direction. Below 48.24 kJ/mol collision energy, in the majority of reactive collisions a relatively long-lived complex (lifetime > 0.5 ps) is formed. The distribution of lifetimes longer than 0.5 ps is close to exponential up to about E_{coll} = 67.5 kJ/mol. This observation is in line with the forward-backward symmetry of the product angular distributions shown in Fig. 6 for low collision energies. At higher collision energies instantaneous reactive collisions dominate. This means that at increasing impact energy the trajectories do not spread within the region of configuration space corresponding to the potential well; instead, they more-or less keep their initial momentum and get out relatively quickly from the well. The inverse of the approximate lifetime of the long-lived reactive complexes, the decay rate constant is in

the range of 7×10^{11} to 2×10^{12} s^{-1} and increases linearly with the collision energy. This is in agreement with the close to linear increase of the excitation function.

The majority of complex-forming collisions are nonreactive. The lifetime distribution of such collision complexes peaks at the first calculated time bin, and only a small fraction of such complexes survive longer than 0.5 ps. Animation of individual trajectories shows that such a short time is enough for the O-H bond to make several oscillations after entering the well across the barrier and before leaving the same way. The decay rate coefficient of the complexes living longer than 0.5 ps is approximately a factor of 3 larger than that of long-lived reactive ones at low collision energies; the factor decreases to 1 when E_{coll} is about 100 kJ/mol. Considering that the energy needed for the complexes to return to reactants is much higher than to decompose to products, this behavior is again an indication that the HO_2 complex does not behave statistically. Another indication comes from the comparison of complex lifetimes when approximately the same amount of total energy is provided in different degrees of freedom (Fig. 13): $v = 0$, $j = 0$, $E_{coll} = 67.5$ kJ/mol or $v = 1$, $j = 0$, $E_{coll} = 49.2$ kJ/mol or $v = 0$, $j = 40$, $E_{coll} = 49.2$ kJ/mol. In addition to the large variation in the magnitude of reactivity, the decay rate of long-lived complexes is smaller if the initial energy comes in the form of vibration and especially of rotation.

CONCLUSIONS

The QCT calculations on the H + $O_2(^1\Delta_g)$ reaction extended the range of initial conditions in the previous quantum scattering calculations to vibrationally and rotationally excited reactants. Both the simple QCT and the GW-QCT methods (see the Methods section) yield excellent agreement with the exact quantum scattering calculations[45] for the excitation function of the reaction of vib-rotationally ground state $O_2(^1\Delta_g)$. Moreover, the product vibrational and rotational distributions also overlap almost perfectly with the exact quantum results. The cross sections proved to be hardly sensitive to vibrational excitation of the

oxygen molecule. Rotational excitation is favorable for the reaction but only a small fraction of the rotational energy is utilized.

The unique nature of the potential energy surface of the reaction, namely, a small barrier in the entrance valley followed by a deep potential well makes the dynamics curious. The expectation based on Polanyi's rule that vibrational energy is less effective than translational at inducing reaction is fulfilled: vibrational excitation does not reduce the threshold energy. Moreover, the vibrational excitation of O_2 is not only not favorable for inducing reaction, but even has an opposite effect: i) above threshold it does slightly reduce the cross sections at the same translational energy even though much larger energy is available for the reactants to cross the barrier and ii) the cross sections significantly decrease when the ratio of vibrational to translational contribution to the same total energy is increased.

After crossing the barrier, for reaction to happen, the system needs to pass the potential well. Out of the collisions getting into the complex region, 80 % return across the barrier and reproduces the reactants, which means that transition state theory cannot be expected to realistically predict the rate of the reaction. The lifetime distribution of collisions shows that reactive trajectories emerge from the potential well with a delay in contrast to the mostly prompt nonreactive complex-forming ones. The lifetime distribution of long-lived HO_2 complexes is close to exponential at low energies, but the decay rate back to the energetically less favorable reactants through the higher barrier is larger than that of decomposition into products. The complex lifetime varies when the initial energy is provided in different degrees of freedom indicating ineffective energy redistribution. From this one can conclude that statistical theory cannot properly describe the behavior of relatively long-lived complexes either. Interestingly, at low collision energy the product angular distributions are forward–backward symmetric because most reactive events involve a long-lived complex, which, however, in this reaction does not mean that the complexes behave statistically.

The thermal rate coefficient (taking into account tunneling) calculated from cross sections agrees well with the measured data of Hack and Kurzke[42] and can be described by the extended Arrhenius form $k_2 = 5.81\times10^{-16}\ T^{1.45}\ \exp(-2270/T)$ cm^3 molecule^{-1} s^{-1} in the temperature range 200-3000 K. Taking into account that the experiments of Cupitt *et al*.[40] and of Basevich and Vedeneev[41] determined the rate of both the reactive and nonreactive quenching of $O_2(^1\Delta_g)$ and obtained almost an order of magnitude larger rate coefficients, one can estimate that the nonreactive quenching is between 12 times (at 300 K) and about 3 times (at about 1000 K) faster than reaction (R2).

Comparison of the reactivity of H atoms with triplet molecular oxygen and $O_2(^1\Delta_g)$ shows that electronic excitation increases the rate coefficient by 4 or 5 orders of magnitude at low temperatures and by about a factor of 10 at high flame temperatures. This means that the presence of singlet molecular oxygen in flames facilitates combustion by increasing the chain-branching step, in agreement with numerous simulations. It should be noted that in combustion modeling, the rate coefficient derived from the measurements of Cupitt *et al*.[40] and of Basevich and Vedeneev[41] is in general use. The current calculations show that these rate coefficients are too large by about an order of magnitude, in agreement with the work of Hack and Kurzke[42]. This means that the simulations applying the rate coefficients including both reaction and electronic quenching in lieu of reaction (2) may overestimate the effect of singlet molecular oxygen on the rate of combustion.

ASSOCIATED CONTENT

Supporting Information

Ref. 3 with complete author list; Figures showing product angular and vib-rotational distributions, rate coefficients for reactions starting from various rotational states of singlet O_2 and versions of Figs. 4, 5 and 11 zoomed at the threshold region. This material is available free of charge via the Internet at http://pubs.acs.org.

AUTHOR INFORMATION

Corresponding Author

* E-mail: lendvay.gyorgy@ttk.mta.hu. Phone +36-1-382-6508

Notes

The authors declare no competing financial interest.

ACKNOWLEDGMENT

We are grateful to Professors Hua Guo and Daiquin Xie for providing us with the potential energy surface code and the quantum dynamical data. This work was supported in part by the Hungarian Scientific Research Fund (Grant No. OTKA T77938 and K108966) and by the National Development Agency (Grant No. KTIA_AIK_12-1-2012-0014 and TÁMOP-4.2.2.A-11/1/KONV-2012-0064).

TABLES

Table 1

Experimental thermal rate coefficients for reaction (R2)

Reaction	A/ $cm^3s^{-1}molecule^{-1}$	E_a / kJ/mol	Temp. range / K	Ref.
(R2) with quenching	1.46×10^{-11}	16.75	300-423	40
(R2) with quenching	1.82×10^{-10}	26.30	520-933	41
(R2) with quenching	6.55×10^{-11}	21.03	300-933	31
(R2)	1.83×10^{-13}	13.00	299-423	42

FIGURE CAPTIONS

Figure 1
The energies (in kJ/mol) of the stationary points of the potential energy surfaces of reactions (R1) (blue) and (R2) (red).

Figure 2
The section of the potential energy surface for reaction (R2) in the H–O–O plane as a function of the location of the H atom with respect to the center of mass of O_2. O_2 is aligned along the *y* axis; its bond length is as specified on each plot. The unit of energy is kJ/mol.

Figure 3
The section of the potential energy surface for reaction (R2) as a function of the length of breaking O–O and of the forming H–O bond. The H–O–O angle is 112.4°. The unit of energy is kJ/mol.

Figure 4

Excitation functions for reactions (R1) and (R2) calculated with exact and statistical quantum mechanical as well as three versions of the quasiclassical trajectory method.

Figure 5
Influence of vibrational and rotational excitation of the reactant $O_2(^1\Delta_g)$ on the excitation function of reaction (R2).

Figure 6
Product angular distribution of reaction (R2) starting from various vib-rotational quantum states of $O_2(^1\Delta_g)$ at several collision energies.

Figure 7
Vibrationally resolved OH rotational distributions in reaction (R2) at two collision energies. For comparison, the distributions obtained in exact quantum mechanical calculations by Ma *et al.* (Ref. 45) are also shown.

Figure 8
Influence of rotational excitation of the reactant $O_2(^1\Delta_g)$ on the thermal rate coefficient of reaction (R2).

Figure 9

Combined (QM + QCT) excitation functions used for tunneling correction at different rotational states of $O_2(^1\Delta_g)$ in the threshold region obtained by merging the classical and QM curves at cross section $\sigma = 0.0335$ Å^2 (indicated by a dotted straight line).

Figure 10
Comparison of the experimental and calculated thermal rate coefficients reaction (R2). The blue dashed line shows the data recommended by Baulch et al.[3] for reaction (R1).

Figure 11
Cross sections characterizing complex formation by H and $O_2(^1\Delta_g)$. See text for details.

Figure 12
Lifetime distribution of complex-forming reactive (closed symbols) and nonreactive collisions in reaction (R2) at various collision energies and reactant quantum states.

Figure 13
Lifetime distribution of complex-forming reactive (closed symbols) and nonreactive collisions in reaction (R2) when the same amount of energy is provided in the translational, vibrational and rotational degrees of freedom, respectively.

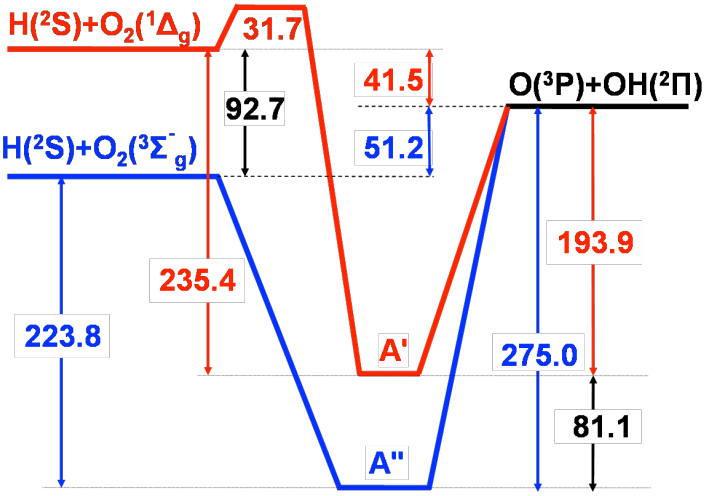

Figure 1
The energies (in kJ/mol) of the stationary points of the potential energy surfaces of reactions (R1) (blue) and (R2) (red).

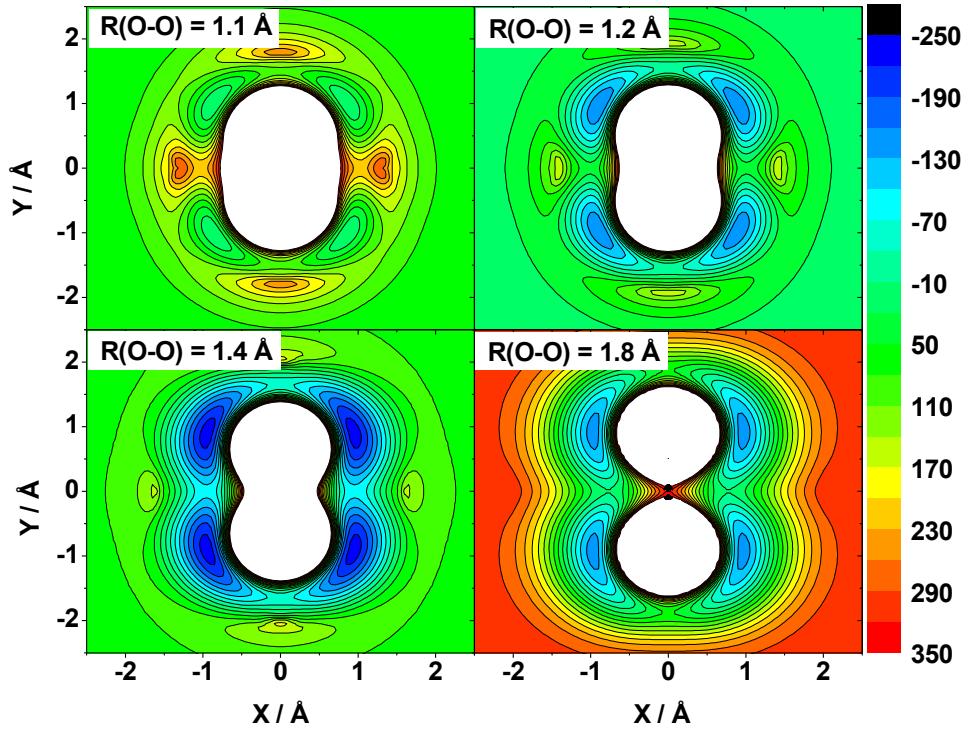

Figure 2
The section of the potential energy surface for reaction (R2) in the H-O-O plane as a function of the location of the H atom with respect to the center of mass of O_2. O_2 is aligned along the *y* axis; its bond length is as specified on each plot. The unit of energy is kJ/mol.

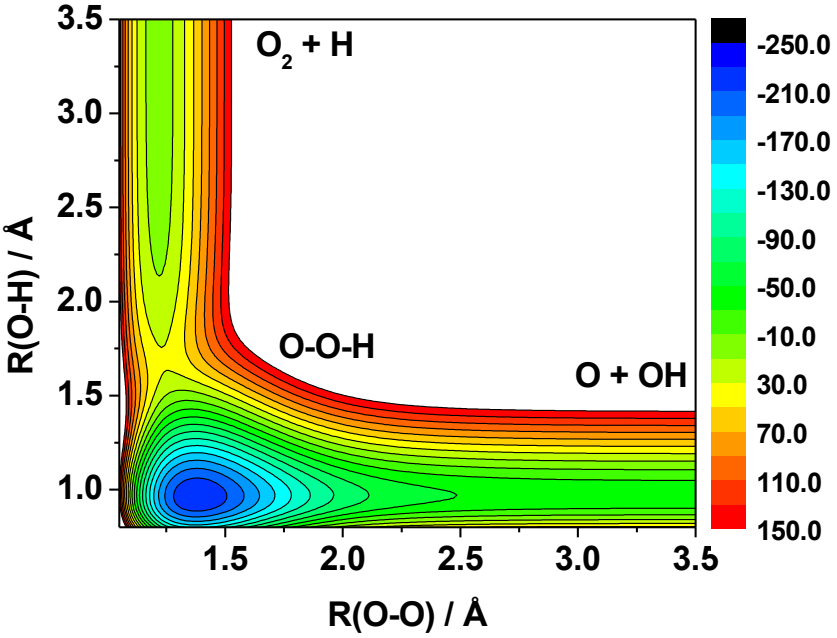

Figure 3
The section of the potential energy surface for reaction (R2) as a function of the length of breaking O–O and of the forming H–O bond. The H–O–O angle is 112.4°. The unit of energy is kJ/mol.

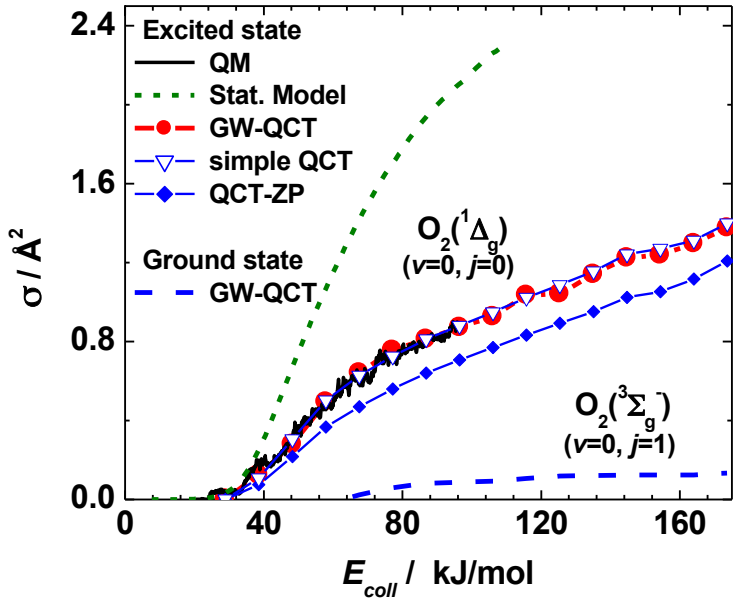

Figure 4

Excitation functions for reactions (R1) and (R2) calculated with exact and statistical quantum mechanical as well as three versions of the quasiclassical trajectory method.

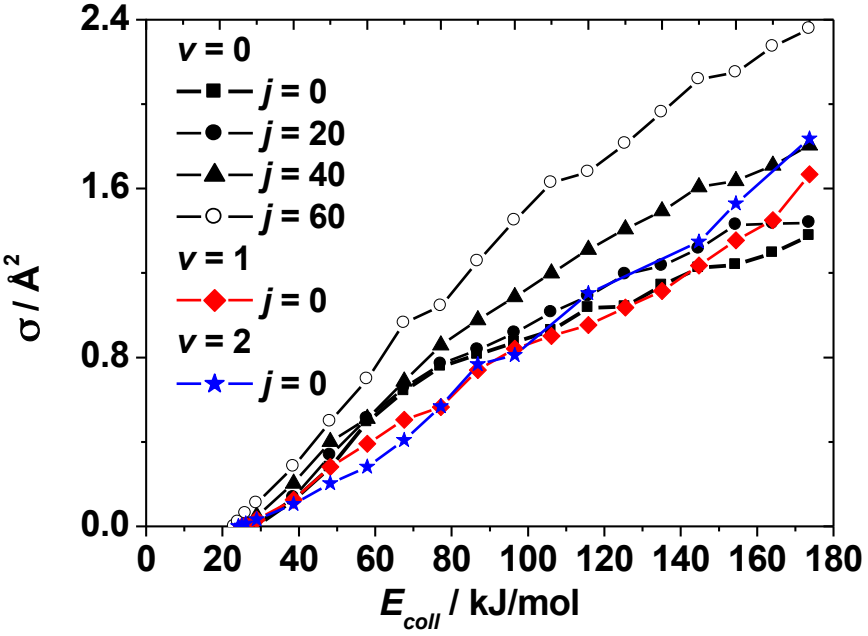

Figure 5
Influence of vibrational and rotational excitation of the reactant $O_2(^1\Delta_g)$ on the excitation function of reaction (R2).

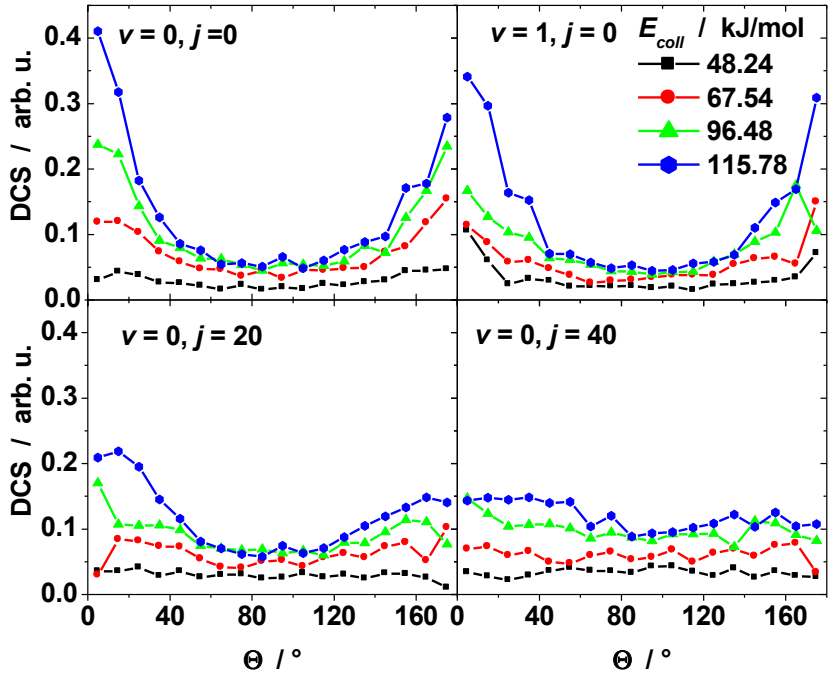

Figure 6
Product angular distribution of reaction (R2) starting from various vib-rotational quantum states of $O_2(^1\Delta_g)$ at several collision energies.

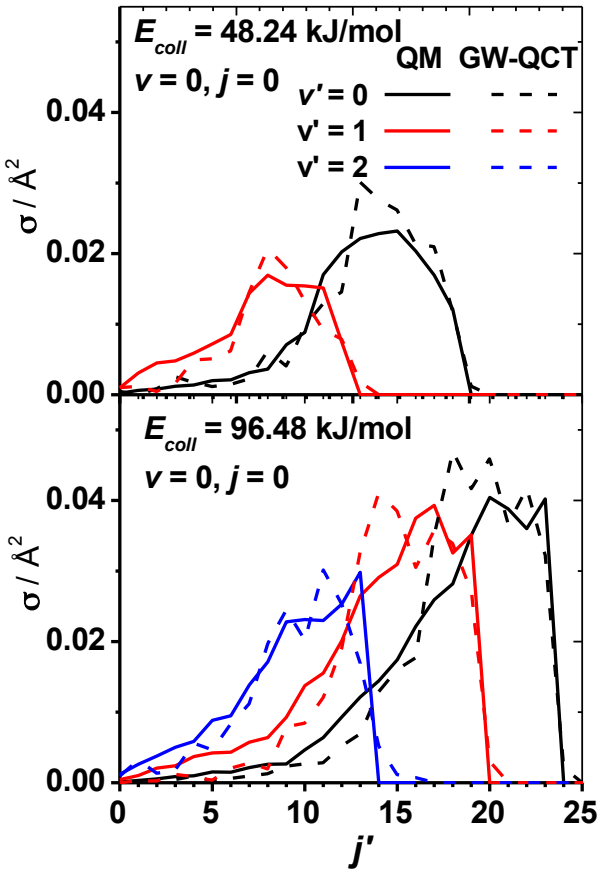

Figure 7
Vibrationally resolved OH rotational distributions in reaction (R2) at two collision energies. For comparison, the distributions obtained in exact quantum mechanical calculations by Ma *et al.* (Ref. 45) are also shown.

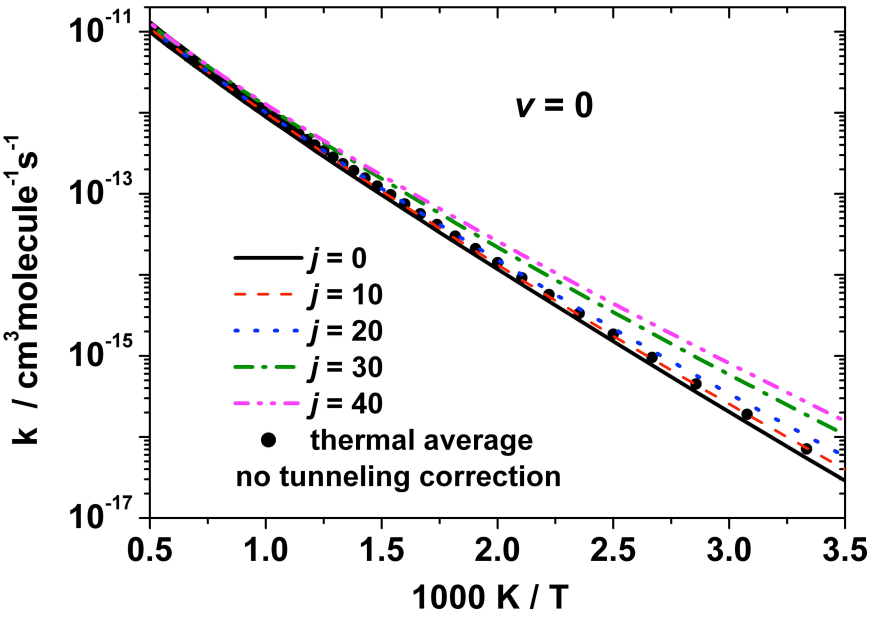

Fig. 8
Influence of rotational excitation of the reactant $O_2(^1\Delta_g)$ on the thermal rate coefficient of reaction (R2).

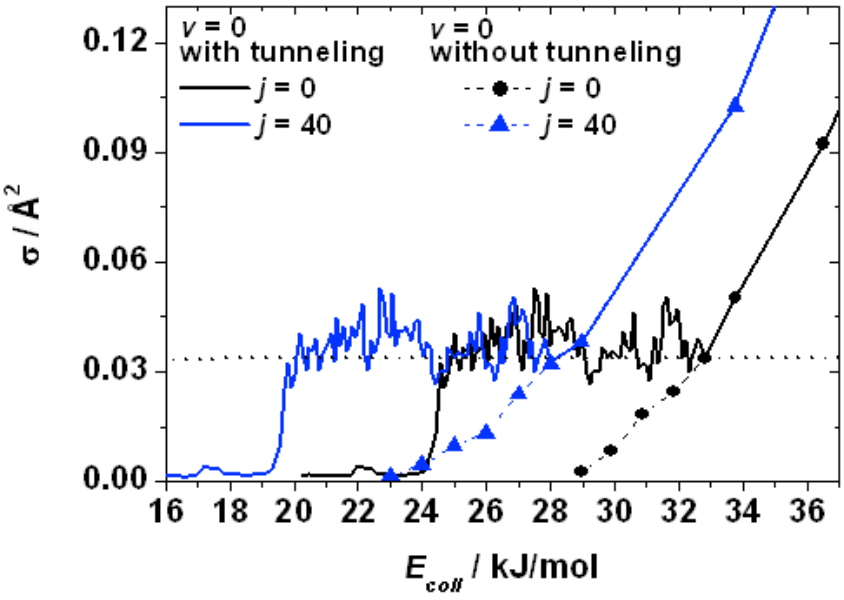

Figure 9

Combined (QM + QCT) excitation functions used for tunneling correction at different rotational states of $O_2(^1\Delta_g)$ in the threshold region obtained by merging the classical and QM curves at cross section $\sigma = 0.0335$ Å^2 (indicated by a dotted straight line).

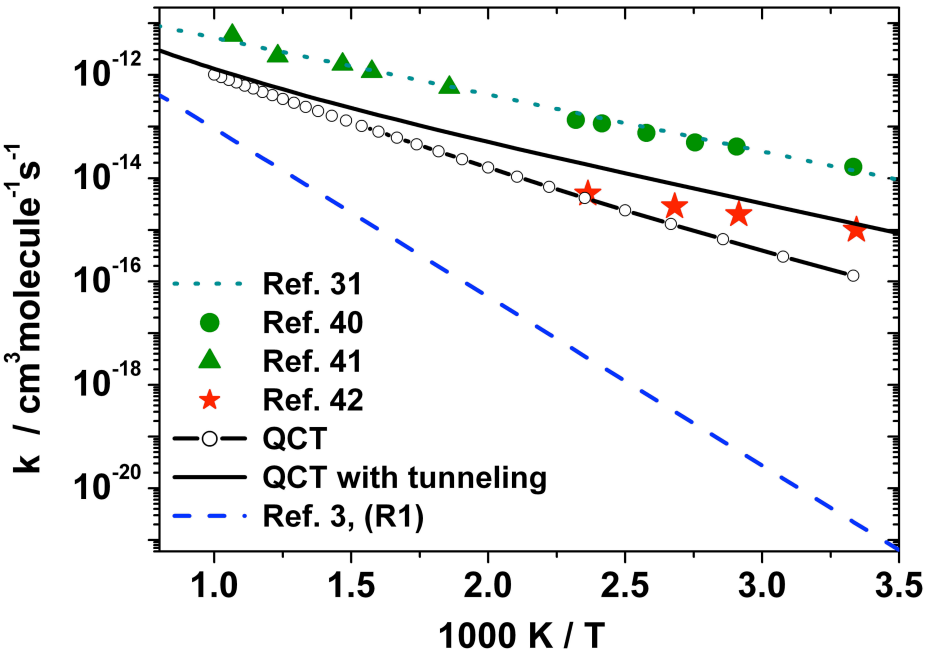

Figure 10
Comparison of the experimental and calculated thermal rate coefficients reaction (R2). The blue dashed line shows the data recommended by Baulch et al.[3] for reaction (R1).

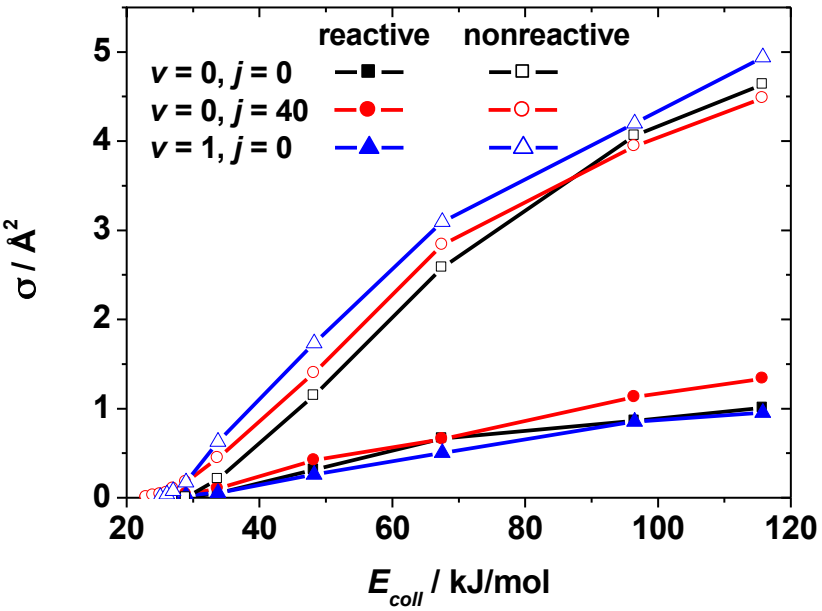

Figure 11
Cross sections characterizing complex formation by H and $O_2(^1\Delta_g)$. See text for details.

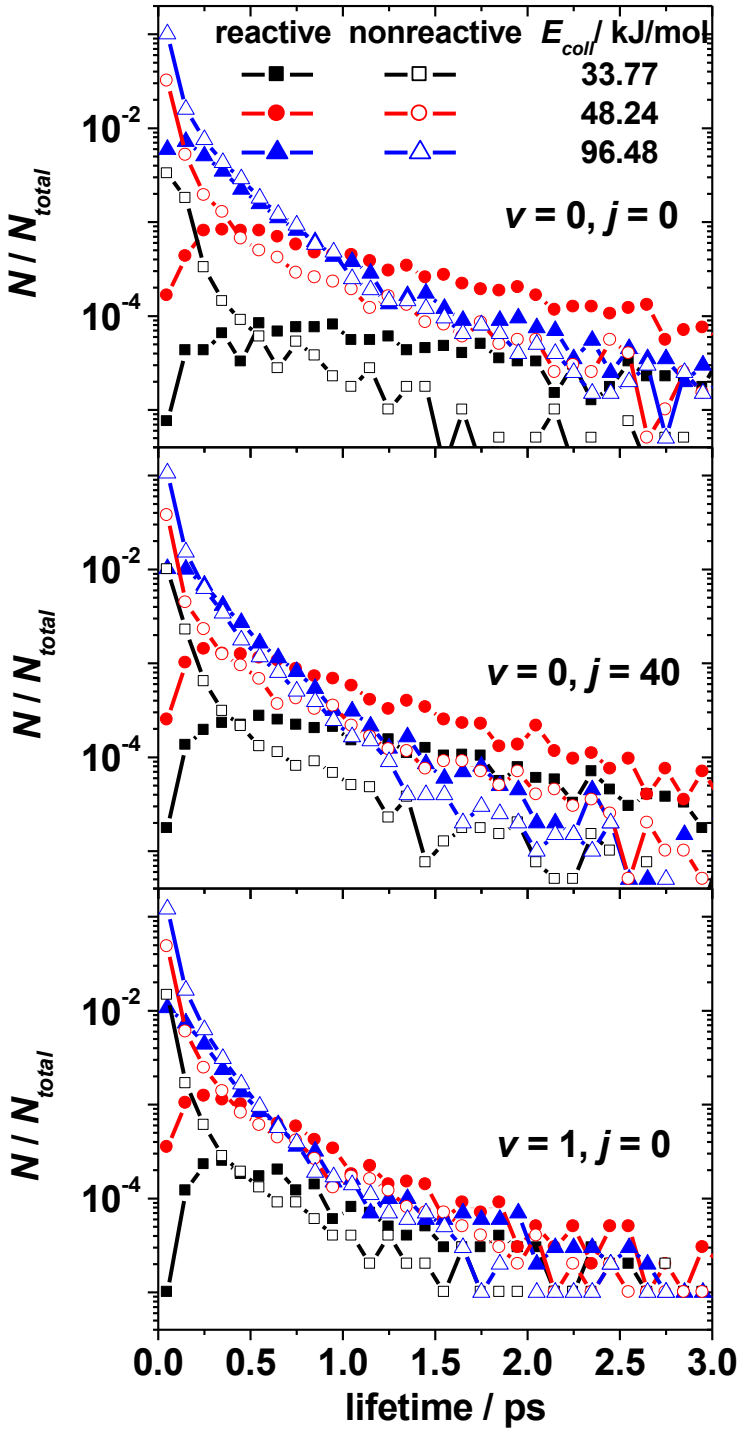

Figure 12
Lifetime distribution of complex-forming reactive (closed symbols) and nonreactive collisions in reaction (R2) at various collision energies and reactant quantum states.

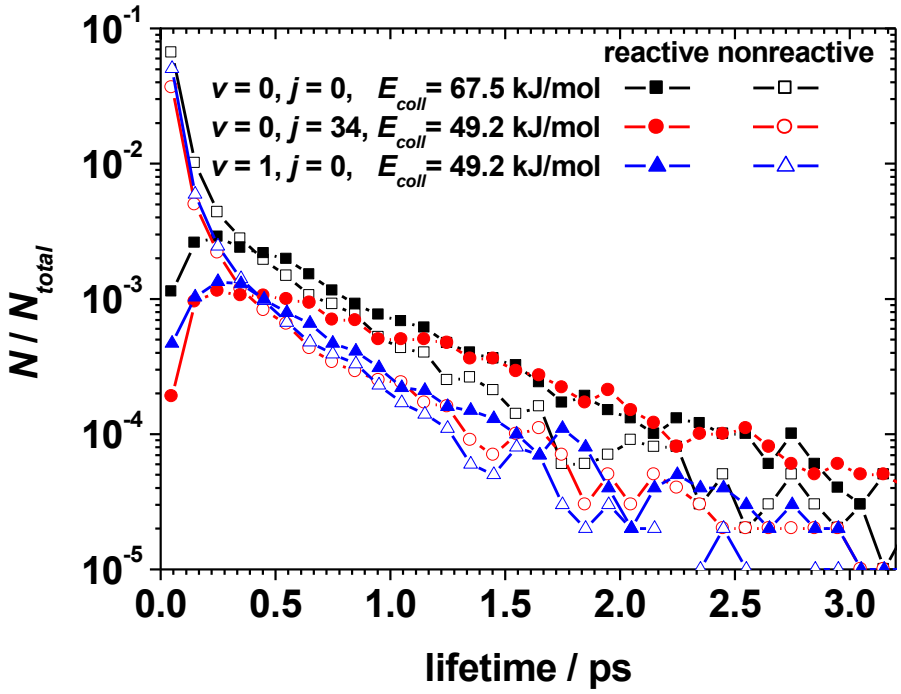

Figure 13
Lifetime distribution of complex-forming reactive (closed symbols) and nonreactive collisions in reaction (R2) when the same amount of energy is provided in the translational, vibrational and rotational degrees of freedom, respectively.

REFERENCES

[1]Miller, J. A.; Kee, R. J.; Westbrook, C. K. Chemical Kinetics and Combustion Modeling, *Annu. Rev. Phys. Chem.* **1990**, *41*, 345-387.

[2]Miller, J. A.; Pilling, M. J.; Troe, J. Unraveling Combustion Mechanisms Through a Quantitative Understanding of Elementary Reactions. *Proc. Combust. Inst.* **2005**, *30*, 43-88.

[3]Baulch, D. L.; Bowman, C. T.; Cobos, C. J.; Cox, R. A.; Just, Th.; Kerr, J.A.; Pilling, M. J.; Stocker, D.; Troe, J.; Tsang. W. et al. Evaluated Kinetic Data for Combustion Modeling: Supplement II. *J. Phys. Chem. Ref. Data* **2005**, *34*, 757-1397.

[4]Pirraglia, A. N.; Michael, J. V.; Sutherland, J. W.; Klemm, R. B. A Flash Photolysis-Shock Tube Kinetic Study of the Hydrogen Atom Reaction With Oxygen: $H + O_2 \leftrightarrow OH + O$ (962 K ≤ T ≤ 1705 K) and $H + O_2 + Ar \rightarrow HO_2 + Ar$ (746 K ≤ T ≤ 987 K). *J. Phys. Chem.* **1989**, *93*, 282–291.

[5]Frank, P.; Just Th. High Temperature Reaction Rate for $H + O_2 = OH + O$ and $OH + H_2 = H_2O + H$. *Ber. Bunsenges. Phys. Chem.* **1985**, *89*, 181-187.

[6]Masten, D. A.; Hanson, R. K.; Bowman, C. T. Shock Tube Study of the Reaction $H + O_2 \rightarrow OH + O$ Using OH Laser Absorption. *J. Phys. Chem.* **1990**, *94*, 7119-7128.

[7]Yuan, T.; Wang, C.; Yu, C.-L.; Frenklach, M.; Rabinowitz, M. J. Determination of the Rate Coefficient for the Reaction Hydrogen Atom + Oxygen → Hydrogen + Oxygen Atom by a Shock Tube/Laser Absorption/Detailed Modeling Study. *J. Phys. Chem.* **1991**, *95*, 1258-1265.

[8]Shin, K. S.; Michael, J. V. Rate Constants for the Reactions H + O_2 → OH + O and D + O_2 → OD + O over the Temperature Range 1085–2278 K by the Laser Photolysis–Shock Tube Technique. *J. Chem. Phys.* **1991**, *95*, 262-273.

[9]Du, H.; Hessler, J. P. Rate Coefficient for the Reaction H + O_2 → OH + O: Results at High Temperatures, 2000 to 5300 K. J. Chem. Phys. **1992**, *96*, 1077-1092.

[10]Hwang, S. M.; Ryu, S.-O.; Witt, K. J.; Rabinowitz, M. J. High Temperature Rate Coefficient Measurements of H+O_2 Chain-Branching and Chain-Terminating Reaction. *Chem. Phys. Letters* **2005**, *408*, 107-111.

[11]Hong, Z.; Davidson, D. F.; Barbour, E. A.; Hanson, R. K. A New Shock Tube Study of the H + O_2 → OH + O Reaction Rate Using Tunable Diode Laser Absorption of H_2O Near 2.5 mm. *Proc. Combust. Inst.* **2010**, *33*, 309-316.

[12]Varandas, A. J. C.; Brandao, J.; Quintales, L. A. M. A Realistic Hydroperoxo ($HO_2(\widetilde{X}\,^2A'')$ Potential Energy Surface from the Double Many-Body Expansion Method. *J. Phys. Chem.* **1988**, *92*, 3732-3742.

[13]Quintales, L. A. M; Varandas, A. J. C; Alvarino, J. M. Quasi-Classical Trajectory Calculations of Thermal Rate for the O + OH → O_2 + H Reaction on Realistic Double Many-Body Expansion Potential-Energy Surface for Ground-State HO_2. *J. Phys. Chem.* **1988**, *92*, 4552-4555.

[14]Varandas, A. J. C. Excitation-Function for H + O_2 Reaction – a Study of Zero-Point Energy Effect and Rotational Distributions in Trajectory Calculations, *J. Phys. Chem.* **1993**, *99*, 1076-1085.

[15]Xie, D.; Xu, C.; Ho, T.-S.; Rabitz, H.; Lendvay, G.; Lin, S. Y.; Guo, H. Global Analytical Potential Energy Surfaces for $HO_2(X^2A")$ Based on High Level Ab Initio Calculations, *J. Chem. Phys.* **2007**, *126*, 074315- 074323.

[16]Harding, L. B.; Maergoiz, A. I.; Troe, J.; Ushakov, V. G. Statistical Rate Theory for the HO + O ⇔ HO_2 ⇔ H + O_2 Reaction System: SACM/CT Calculations Between 0 and 5000 K. *J. Chem. Phys.* **2000**, *113*, 11019-11034.

[17]Troe, J.; Ushakov, V. G. Theoretical Studies of the HO + O ⇔ HO_2 ⇔ H + O_2 Reaction. II. Classical Trajectory Calculations on an Ab Initio Potential for Temperatures Between 300 and 5000 K. *J. Chem. Phys.* **2001**, *115*, 3621-3628.

[18]Harding, L. B.; Troe, J.; Ushakov, V. G. Classical Trajectory Calculations of the High Pressure Limiting Rate Constants and of Specific Rate Constants for the Reaction H + O_2 → HO_2: Dynamic Isotope Effects Between Tritium+ O_2 and Muonium + O_2. *Phys. Chem. Chem. Phys.* **1999**, *2*, 631-642.

[19]Michael, J. V.; Sutherland, J. W.; Harding, L. B.; Wagner, A. F. Initiation in H_2/O_2: Rate Constants for H_2 + O_2 → H + HO_2 at High Temperature. *Proc. Comb. Inst.* **2000**, *28*, 1471–1478.

[20]Troe, J. The Struggle for Precise Rate Constants in Gas Phase Reaction Kinetics: the Reaction H + O_2 ⇔ HO + O. *Z. Phys. Chem.* **2003**, *217*, 1303–1317.

[21]Lendvay, G.; Xie, D.; Guo, H.; Mechanistic Insights into the H + O_2 → OH + O Reaction from Quasi-Classical Trajectory Studies on a New Ab Initio Potential Energy Surface, *Chem. Phys.* **2008**, *349*, 181–187.

[22]Sun, Z.; Zhang, D. H.; Xu, C.; Zhou, S.; Xie, D.; Lendvay, G.; Lee, S.-Y.; Lin, S.Y.; Guo, H. State-to-State Dynamics of H + O_2 Reaction, Evidence for Nonstatistical Behavior, *J. Am. Chem. Soc.* **2008**, *130*, 14962-14963.

[23]Lin, S. Y.; Xie, D.; Guo, H. Revelation of Non-Statistical Behavior in HO_2 Vibration by a New Ab Initio Potential Energy Surface, *J. Chem. Phys.* **2006**, *125*, 091103-091103-4.

[24]Guo, H. Quantum Dynamics of Complex-Forming Reactions. *Int. Rev. Phys. Chem.* **2012**, *31*, 1-68.

[25]Lin, S. Y.; Guo, H.; Honvault, P.; Xie, D. Quantum Dynamics of the H + O_2 → O + OH Reaction on an Accurate Ab Initio Potential Energy Surface. *J. Phys. Chem. B.* **2006**, *110*, 23641-23643.

[26]Honvault, P.; Lin, S. Y.; Xie, D.; Guo, H. Differential and Integral Cross Sections for the H + O_2 → HO + O Combustion Reaction. *J. Phys. Chem. A.* **2007**, *111*, 5349-5352.

[27]Lin, S. Y.; Sun, Z.; Guo, H.; Zhang, D. H.; Honvault, P.; Xie, D.; Lee, S.-Y. Fully Coriolis Coupled Quantum Studies of the H + O_2 (v_i=0-2, j_i=0,1) → OH + O Reaction on an Accurate Potential Energy Surface: Integral Cross Sections and Rate Constants. *J. Phys. Chem. A.* **2008**, *112*, 602-611.

[28]Basevich, V. Ya.; Kogaro, S. M., O Mekhanizme Vliyaniya Produktov Tleyushchego Razryada na Skorost' Vodorodno-Kislorodnikh Plamen v Usloviyah Poluostrova Vosplameneniya [On the Mechanism of the Products of Glow Discharge on the Rate of Hydrogen-Oxygen Flames under the Conditions of the Ignition Peninsula] *Kinet. Katal.* **1966**, *7*, 393-401.

[29]Huber, K. P.; Herzberg, G. Molecular Spectra and Molecular Structure IV. Constants of Diatomic Molecules. New York: Van Nostrand Reinhold, 1979.

[30]Sandor, B. J.; Clancye, R. T.; Rusch, D. W.; Randall, C. E.; Eckrnan, R. S.; Siskind, D. S.; Muhleman, D. O. Microwave Observations and Modeling of $O_2(^1\Delta_g)$ and O_3 Diurnal Variation in the Mesosphere, *J. Geophys. Res.* **1997**, *102*, 9013-9028.

[31]Popov, N. A. The Effect of Nonequilibrium Excitation on the Ignition of Hydrogen-Oxygen Mixtures. *High Temp.* **2007**, *45*, 261-279.

[32]Bourig, A.; Thévenin, D.; Martin, J.-P.; Janiga, G.; Zähringer, K. Numerical Modeling of H_2–O_2 Flames Involving Electronically-excited Species ($a^1\Delta_g$), $O(^1D)$ and $OH(^2\Sigma^+)$, *Proc. Combust. Inst.* **2000**, *28*, 1471-1478.

[33]Ombrello, T.; Wona, S. H.; Jua, Y. Flame Propagation Enhancement by Plasma Excitation of Oxygen. Part II: Effects of $O_2(a^1\Delta_g)$. *Combust. Flame* **2010**, *157*, 1906-1915.

[34]Basevich, V. Ya.; Belyaev, A. A.; Raschet Uvelicheniya Skorosti Vodorodno-Kislorodnogo Plameni Pri Dobavki Singletnogo Oxigena [Calculation of the Enhancement of the Rate of Hydrogen-Oxygen Flames by Addition of Singlet Oxygen] *Khim. Fiz.* **1989**, *8*, 1124-1129.

[35]Chukalovsky, A. A.; Rakhimova, T. V.; Klopovsky, K. S.; Popov, N. A.; Mankelevich, Yu. A.; Proshina, O. V.; Specific Features of the Kinetics of H_2–O_2–$O_2(a^1\Delta_g)$ Mixtures: I. Formation and Quenching of Electronically and Vibrationally Excited HO_2*(A') Molecules in H_2–O_2–$O_2(a^1\Delta_g)$ Mixtures at a Temperature of 300 K, *Plasma Phys. Rep.* **2014**, *40*, 34–51.

[36]Smirnov, V. V.; Stelmakh, O. M.; Fabelinsky, V. I.; Kzolov, D. N.; Starik, A. M.; Titova, N. S. On the Influence of Electronically Excited Oxygen Molecules on Combustion of Hydrogen–Oxygen Mixture *J. Phys, D: Appl. Phys*. **2008**, *41*, 192001-192007.

[37]Brown, R. L. An Upper Limit for the Rate of Destruction of $O_2(^1\Delta_g)$ by Atomic Hydrogen, *J. Geophys. Res. Space Phys*. **1970**, *75*, 3935-3936.

[38]Westenberg, A. A.; Roscoe, J. M.; DeHaas, N. Rate Measurement on $N + O_2(a^1\Delta_g) \rightarrow NO + O$ and $H + O_2(a^1\Delta_g) \rightarrow OH + O$. *Chem. Phys. Lett*. **1970**, *7*, 597-599.

[39]Schmidt, C.; Schiff, H. I. Reactions of Singlet Oxygen with atomic Nitrogen and Hydrogen, *Chem. Phys. Lett*. **1973**, *23*, 339-342.

[40]Cupitt, L. T.; Takacs, G. A.; Glass G. P. Reaction of Hydrogen Atoms and $O_2(^1\Delta_g)$, *Int. J. Chem. Kinet. 1982*, **14**, 487-497.

[41]Basevich, V. Ya.; Vedeneev, V. I.; Konstanta Skorost'i Reakcii $H + O_2(^1\Delta) = OH + O$ [The Rate Constant of the $H + O_2(^1\Delta) = OH + O$ Reaction] *Khim. Fiz*. **1985**, *4*, 1102-1108.

[42]Hack, W.; Kurzke, H. Kinetic Study of the Elementary Chemical Reaction $H(^2S_{1/2}) + O_2(^1\Delta_g) \rightarrow OH(^2\Pi) + O(^3P)$ in the Gas Phase, *J. Phys. Chem*. **1986**, *90*, 1900-1906.

[43]Starik, A. M.; Titova, N. S. Possibility of Initiation of Combustion of CH_4–O_2 (Air) Mixtures with Laser-Induced Excitation of O_2 Molecules. *Combustion, Explosion, and Shock Waves*, **2004**, *40*, 499–510.

[44]Li, A.; Xie, D.; Dawes, R.; Jasper, A. W.; Ma, J.; Guo, H. Global potential energy surface, vibrational spectrum, and reaction dynamics of the first excited (A^2A') state of HO_2. *J. Chem. Phys*. **2010**, *133*, 144306-144314.

[45]Ma, J.; Guo, H.; Xie, C.; Li, A.; Xie, D. State-to-state Quantum Dynamics of the $H(^2S)$ + $O_2(a^1\Delta_g) \rightarrow O(^3P) + OH(X^2P)$ Reaction on the First Excited State of $HO_2(A^2A')$. *Phys. Chem. Chem. Phys.* **2011**, *13*, 8407-8413.

[46]Polanyi, J. C. Concepts in Reaction Dynamics. *Acc. Chem. Res.* **1972**, *5*, 161-168.

[47] Hase W. L., Duchovic R. J., Lu D.-H., Swamy K. N., Vande Linde S. R., Wolf R. J.; VENUS, a General Chemical Dynamics Computer Program; 1988.

[48]Banares, L.; Aoiz, F. J.; Honvault, P.; Bussery-Honvault, B., Launay, J.-M. Quantum Mechanical and Quasi-classical Trajectory Study of the $C(^1D) + H_2$ Reaction Dynamics *J. Chem. Phys.* **2003**, *118*, 565-568.

[49]Bonnet, L.; Rayez, J.-C. Quasiclassical Trajectory Method for Molecular Scattering Processes: Necessity of a Weighted Binning Approach, *Chem. Phys. Lett.* **1997**, *277*, 183-190.

[50]Bonnet, L.; Rayez, J.-C. Gaussian Weighting in the Quasiclassical Trajectory Method, *Chem. Phys. Lett.* **2004**, *397*, 106-109.

[51]Rackham, E. J.; Huarte-Larranaga, F.; Manolopoulos, D. E. Coupled-channel Statistical Theory of the $N(^2D) + H_2$ and $O(^1D) + H_2$ Insertion Reactions, *Chem. Phys. Lett.* **2001**, *343*, 356-364.

[52]Rackham, E. J.; Gonzalez-Lezana, T.; Manolopoulos, D. E. A Rigorous Test of the Statistical Model for Atom-Diatom Insertion Reactions, *J. Chem. Phys.* **2003**, *119*, 12895-12907.

[53] Forst, W, Theory of Unimolecular Reactions; Academic Press: New York, **1973**

[54]Smith, F.T. Lifetime Matrix in Collision Theory. *Phys. Rev.* **1960**, *118*, 349-356.

Graphical Abstract